Title

Sequence-Dependent Self-Assembly and Structural Diversity of Islet Amyloid Polypeptide-Derived β-Sheet Fibrils

Journal

ACS Nano, 11(9)

ISSN

1936-0851

Authors

Wang, Shih-Ting
Lin, Yiyang
Spencer, Ryan K
et al.

Publication Date

2017-09-26

DOI

10.1021/acsnano.7b02325

Peer reviewed

ACS NANO

www.acsnano.org

ARTICLE

Sequence-Dependent Self-Assembly and Structural Diversity of Islet Amyloid Polypeptide-Derived β-Sheet Fibrils

Shih-Ting Wang,[†] Yiyang Lin,[†] Ryan K. Spencer,[‡] Michael R. Thomas,[†] Andy I. Nguyen,[‡] Nadav Amdursky,[†] E. Thomas Pashuck,[†] Stacey C. Skaalure,[†] Cheng Yu Song,[‡] Paresh A. Parmar,[†] Rhodri M. Morgan,[§] Peter Ercius,[‡] Shaul Aloni,[‡] Ronald N. Zuckermann,[‡] and Molly M. Stevens*[,†]

[†]Department of Materials and Department of Bioengineering and Institute of Biomedical Engineering, Imperial College London, Exhibition Road, London SW7 2AZ, United Kingdom

[‡]Molecular Foundry, Lawrence Berkeley National Laboratory, 1 Cyclotron Road, Berkeley, California 94720, United States

[§]Department of Life Sciences, Imperial College London, Exhibition Road, London SW7 2AZ, United Kingdom

Supporting Information

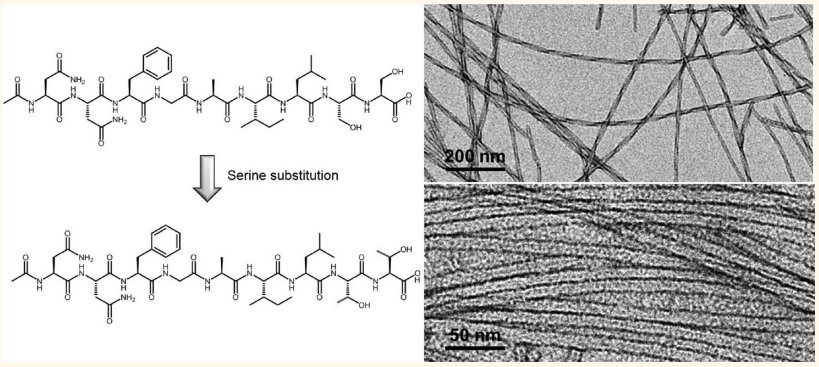

ABSTRACT: **Determining the structural origins of amyloid fibrillation is essential for understanding both the pathology of amyloidosis and the rational design of inhibitors to prevent or reverse amyloid formation. In this work, the decisive roles of peptide structures on amyloid self-assembly and morphological diversity were investigated by the design of eight amyloidogenic peptides derived from islet amyloid polypeptide. Among the segments, two distinct morphologies were highlighted in the form of twisted and planar (untwisted) ribbons with varied diameters, thicknesses, and lengths. In particular, transformation of amyloid fibrils from twisted ribbons into untwisted structures was triggered by substitution of the C-terminal serine with threonine, where the side chain methyl group was responsible for the distinct morphological change. This effect was confirmed following serine substitution with alanine and valine and was ascribed to the restriction of intersheet torsional strain through the increased hydrophobic interactions and hydrogen bonding. We also studied the variation of fibril morphology (*i.e.*, association and helicity) and peptide aggregation propensity by increasing the hydrophobicity of the peptide side group, capping the N-terminus, and extending sequence length. We anticipate that our insights into sequence-dependent fibrillation and morphological diversity will shed light on the structural interpretation of amyloidogenesis and development of structure-specific imaging agents and aggregation inhibitors.**

KEYWORDS: *amyloid fibrils, islet amyloid polypeptide, helical nanostructures, self-assembly, nanoribbons*

Undesired amyloid fibrillation is associated with serious pathogeneses of neurodegenerative disorders (*e.g.*, Alzheimer's, Huntington's, Parkinson's diseases, prion encephalopathies) and progressive diseases (*e.g.*, type II diabetes, light chain amyloidosis, and cystic fibrosis).[1,2] Amyloid fibrillation arises from a misfolding process in which proteins undergo a 3D structural conversion from their native form (often soluble) into insoluble fibrillar aggregates.[3] Although amyloid fibrils share a common structural feature based on the continuous stacking of β-sheets, known as the cross-β structure,[4,5] diverse fibril structures (*i.e.*, polymorphs) can be formed *via* different energy transduction pathways during supramolecular organization.[6,7] Depending on the

Received: April 3, 2017
Accepted: July 28, 2017
Published: August 3, 2017

DOI: 10.1021/acsnano.7b02325
ACS Nano 2017, 11, 8579–8589

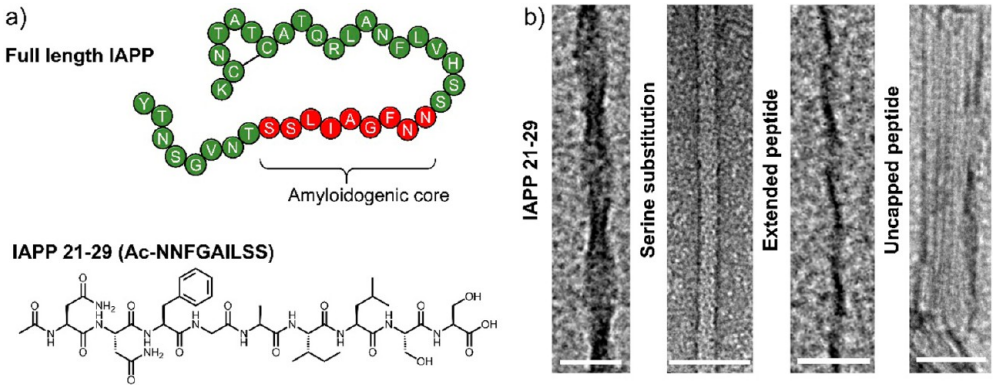

Figure 1. (a) Sequence of full-length IAPP (1−37 residues) and its amyloidogenic core (21−29 residues, Ac-NNFGAILSS). (b) Negative stained TEM images of the polymorphic amyloid structures including twisted and planar ribbons of different sizes (left to right: Ac-NNFGAILSS, Ac-NNFGAILTT, Ac-SSNNFGAILSS, H-SSNNFGAILSS). Scale bar: 50 nm.

species, amyloid peptides/proteins display structural diversity under certain physicochemical conditions, which is related to a variety of disease strains and phenotypes. For example, distinct "daughter" fibril morphologies and neuronal toxicities of amyloid β (Aβ) associated with Alzheimer's disease have been observed through seeding with selective "parent" seeds, which may have implications for different strains or pathological manifestations.[8] Understanding amyloid pathways and their possible conformations that could lead to pathogenesis and degeneration is a vital area of research.

Similar to naturally occurring proteins, short amyloid fragments can also exhibit polymorphic β-sheet structures when subtle structural modifications are applied.[9−11] This includes variation of environmental conditions and changing of amino acid sequences (*e.g.*, single atom replacement of hydrogen to halogen, incorporation of β-amino acids or aromatic residues, rearrangement of the hydrophobic/hydrophilic residues).[12−21] This is due to the multiple noncovalent interactions involved in determining a cross-β structure such as hydrogen bonds (H-bonds), hydrophobic interactions, electrostatic attractions, van der Waals forces, and $\pi-\pi$ interactions.[4,5,12,13,22−26] For example, Castelletto *et al.* showed that the formation of helical ribbon nanostructures by substitution of the α-alanine residues with β-alanine in the extended Aβ variant sequence (AAKLVFF), which was different to the cylindrical fibrils (KLVFF) or twisted tapes (AAKLVFF) reported in other works.[17] Hu *et al.* reported the important role of electrostatic repulsions between terminal charges in mediating the transformation from twisted ribbons into laminated nanobelts.[12] Coassembly of oppositely charged amyloid-inspired peptides into cylindrical nanostructures based on electrostatic attraction was reported by Cinar and colleagues.[25] Liang *et al.* reported a morphological transition of Aβ (16−22), Ac-KLVFFAE-NH_2, from hollow nanotubes into fibers following the changes in β-strand registry at different pH conditions.[20] Because amyloid fragments share similar self-assembly mechanisms with natural proteins, an investigation of their structural diversities will contribute to the understanding into amyloid-related biological processes.

In this work, we sought to determine the effect of amino acid sequences on the self-assembly behavior and fibril morphology of amyloidogenic peptides derived from islet amyloid polypeptide (IAPP), a 37 amino acid peptide hormone co-secreted with insulin to regulate the glucose levels.[27,28] The susceptibility to IAPP fibrillation due to the presence of a hydrophobic core has been implicated in type II diabetes through the deposition of amyloid plaques.[29] Herein, a series of amyloidogenic segments derived from the 21−29 residues of IAPP (Ac-NNFGAILSS) was designed, and the structures of amyloid fibrils were systematically characterized using transmission electron microscopy (TEM), scanning transmission electron microscopy (STEM), X-ray diffraction (XRD), atomic force microscopy (AFM), Thioflavin T (ThT) fluorescence assay, and circular dichroism (CD). By tailoring the amino acid residues at the C-terminal domain (Ser28, Ser29), which have been shown to determine the fibrillation of the hydrophobic core sequence (IAPP 20−29 residues),[30] we demonstrated the importance of H-bonds and side chain interactions in regulating peptide fibrillation and stabilizing distinct amyloid structures. In particular, we presented the formation of periodically twisted nanoribbons by Ac-NNFGAILSS, where different sizes of nanoribbons corresponding to the numbers of associated fibrils were observed. By tailoring the amino acid substitutions and sequence lengths, polymorphic fibrils were observed in a series of IAPP-derived fragments, where a correlation between molecular interactions and fibril helicity was hypothesized to emphasize the role of conformational constraints. The effects of N-terminal acetylation and sequence elongation on β-sheet strength, peptide hydrogelation, and fibril morphology were also studied. We anticipate our findings can help to understand the sequential determinants toward peptide self-assembly and amyloid polymorphism.

RESULTS AND DISCUSSION

Atomic structures obtained from the microcrystals of IAPP 21−27 residues (NNFGAIL) revealed a tight main chain interaction between β-sheet layers.[31] This observation inspired us to investigate the morphological variability of peptides derived from the amyloidogenic core. We designed eight peptide sequences by tailoring the terminal residues (*i.e.*, substitution, elongation, N-terminal capping/uncapping) derived from Ac-NNFGAILSS (Figure 1a), including Ac-NNFGAILTT, Ac-NNFGAILAA, Ac-NNFGAILVV, Ac-SSNNFGAIL, Ac-SSNNFGAILSS, Ac-TTNNFGAILTT, and H-SSNNFGAILSS, and studied the structural polymorphs of amyloid fibrillation (Figure 1b). Two major morphologies, the twisted and planar ribbons, were presented by tailoring the amino acid sequences. Polymorphic structures depending on the number of associated fibrils and β-sheet stacking that resulted in thin or thick ribbons were also investigated.

DOI: 10.1021/acsnano.7b02325
ACS Nano 2017, 11, 8579−8589

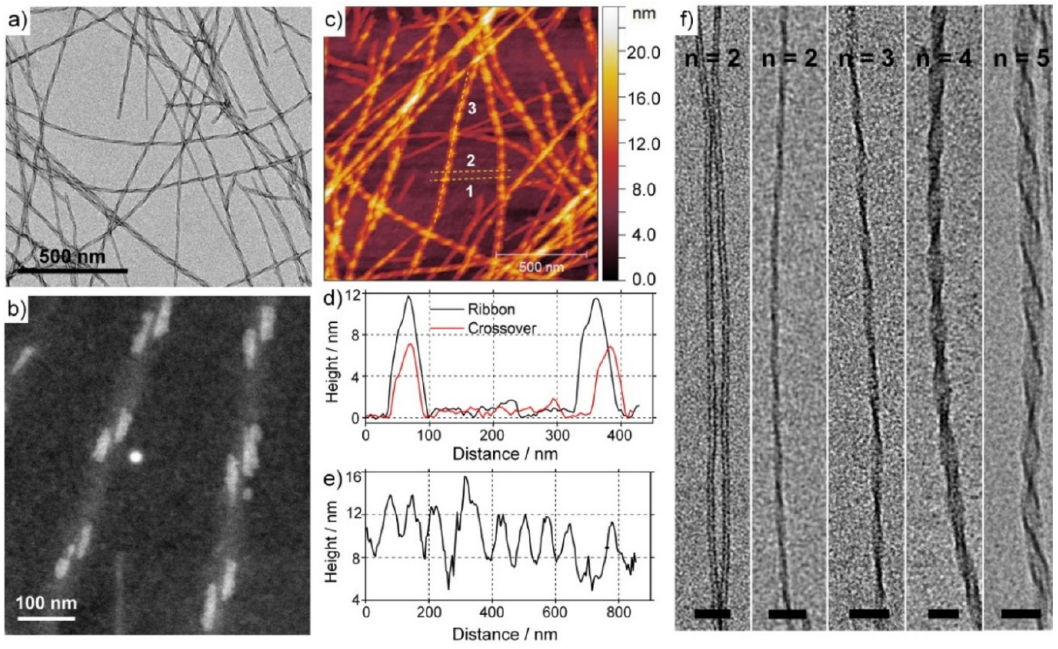

Figure 2. Structural characterizations of Ac-NNFGAILSS ribbons. (a) Negative stained TEM and (b) unstained HAADF-STEM images showing the twisted structure of Ac-NNFGAILSS ribbons. (c–e) AFM image revealing the topography of Ac-NNFGAILSS ribbons. The height profiles of (d) thickness at the ribbon 1, crossover 2, and (e) spacing between crossovers 3 were plotted along the yellow dashed lines and labeled in image (c). (f) Negative stained TEM images showing the different sizes of the Ac-NNFGAILSS ribbons, which corresponded to the different numbers of associated fibrils. Scale bar: 50 nm.

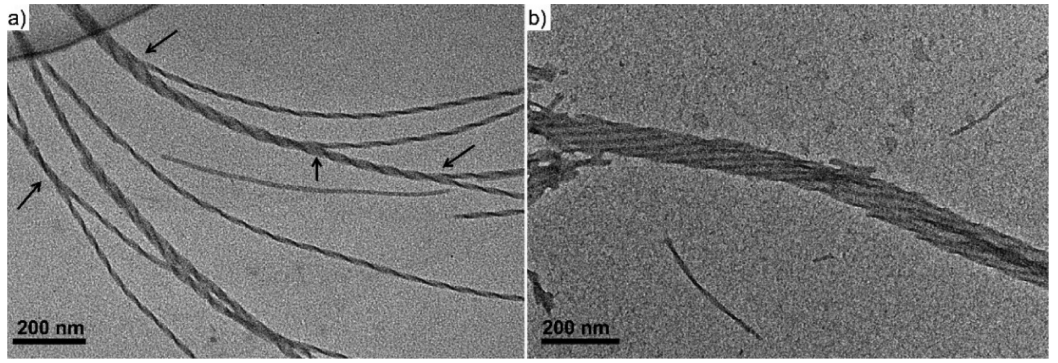

Figure 3. TEM images showing the aggregation of twisted Ac-NNFGAILSS ribbons into superhelical structures. (a) Large superhelices were formed by interwound helices composed by three individual fibrils. (b) Superhelix consisting of n = 14 fibrils (diameter: 83.0 nm) with a tilt angle (γ) of 13.7°.

As shown in Figure 2a, amyloid fibrils obtained from Ac-NNFGAILSS exhibited twisted ribbon-like structures with distinct axial periodicities (pitch: 85–100 nm). The high-angle annular dark-field (HAADF)-STEM image recorded a high-contrast image of the amyloid fibrils (Figures 2b and S1), where the strong scattering from the residual salts of the sodium phosphate buffer "stained" the ribbons and confirmed the diameters of uranyl acetate-stained fibrils obtained from TEM imaging. AFM topographic imaging (Figure 2c–e) revealed that the ribbon thickness was 11.4 nm and the height at the crossover was 6.4 nm. This agreed with the diameter measured from TEM imaging, in which the average size of individual fibrils was approximately 5–6 nm (Figure S2). The length of the Ac-NNFGAILSS peptide was estimated to be approximately 3.4 nm using PyMOL software. Based on these findings, it was concluded that an individual fibril consisted of two adjacent β-sheets, with the hydrophobic inner surfaces packed tightly against each other.

Ribbon-like structures in Ac-NNFGAILSS exhibited different sizes based on the number of associated fibrils (Figure 2f). The smallest peptide ribbon had two fibrils (n = 2) aligned side-by-side or in a twisted orientation, with diameters of 10.2 and 11.7 nm, respectively. Most twisted nanoribbons had a diameter of 14–16 nm, which corresponded to the association of three fibrils (n = 3). As shown in Figure S3, the nanoribbons exhibited a periodical spacing of 93.4 nm, which was consistent with the AFM result (Figure 2e). Such large spacing has frequently been seen when fibrils are loosely coiled, implicating the flexibility of intersheet interactions.[32] Larger ribbons with diameters of 24.4 and 30.2 nm and periodical spacing of 97.6 and 88.2 nm corresponded to the association of n = 4 and n = 5 fibrils, respectively.

The periodical spacing of these larger ribbons remained at 85–100 nm, which was similar to those of the smaller Ac-NNFGAILSS ribbons composed primarily of three fibrils. In fact, bundle formation of β-sheet-forming peptides with finite

DOI: 10.1021/acsnano.7b02325
ACS Nano 2017, 11, 8579–8589

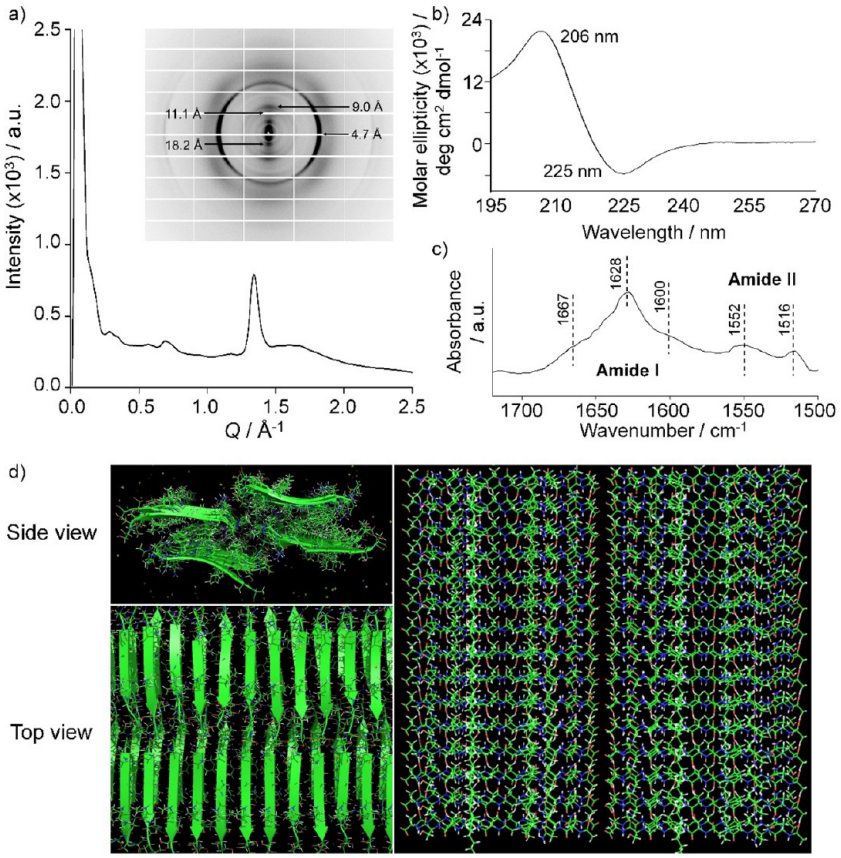

Figure 4. Structural characterization of the Ac-NNFGAILSS ribbons. (a) XRD of the dried stalk of Ac-NNFGAILSS ribbon showing the typical interstrand and intersheet spacing of 4.7 and 11.1 Å, respectively. (b) CD and (c) Fourier transform infrared spectra of the Ac-NNFGAILSS ribbons. Peaks in the amide I and amide II regions are labeled in (c), suggesting the formation of the parallel β-sheet structure. (d) Structure of Ac-NNFGAILSS ribbons depicted using PyMol software. Upper left: side view. Lower left: top view. Right: predicted 3D β-sheet structure.

fibril width and helicity has been reported to stem from a competition between free energy gain from attraction between ribbons and penalty due to elastic distortion from the further growth of intrinsically twisted ribbons.[33−35] These suggested that the larger ribbons were formed by bundling two or more smaller ribbons during the aging process (Figure 3a). In addition, right-handed helical structures were found in higher-order twisted structures (Figures 2d and 3b); for example, a tilt angle (γ) of n = 5 ribbons was estimated to be 17.7° (Figure 2d). Formation of superhelical structures resembled the quadruple helix reported by Muraoka *et al.*, in which the helix was composed of two smaller helices, each of which was composed of two individual fibrils.[36] Given that fibril association is a time-dependent and self-propagating process that forms the final energy-favorable structures,[32,37] the growth of Ac-NNFGAILSS fibril was further examined at different time points. As shown in Figure S4, no noticeable twisted ribbons were observed within 6 h, whereas elongated twisted fibrils formed with the increasing aging time. The majority of twisted ribbons were seen to favor an association of n = 3 fibrils over time, suggesting that this was the most thermodynamically stable structure for the Ac-NNFGAILSS assembly.

The kinetics of β-sheet formation by Ac-NNFGAILSS was analyzed by ThT fluorescence assay, where the sigmoidal-shaped profile was noted in the process of peptide fibrillation (Figure S5). The role of β-sheets was highlighted through the addition of high concentration of urea (4 M) to break the H-bonding networks and weaken the β-sheet structures; this not only reduced the number of mature Ac-NNFGAILSS ribbons, but they were also less twisted (Figure S6). The microcrystal structure of Ac-NNFGAILSS β-sheet structure was obtained by XRD using a dried aligned stalk that was mounted in parallel with the X-ray beam. The 2D diffraction pattern showed a strong meridional reflection at 4.7 Å, which corresponded to the spacing between H-bonded β-strands within a β-sheet (Figure 4a). The equatorial rings at ∼10 Å (with two concentric rings at 11.1 and 9.0 Å) and 18.2 Å corresponded to the short- and long-range intersheet distances, respectively. Multiple concentric rings (*i.e.*, 9.0 and 11.1 Å) have been seen in thick amyloid fibers consisting of either two or more concentric cylindrical β-sheets or two or more single cylindrical fibers wound around each other.[38] This was in agreement with the varied sizes of Ac-NNFGAILSS nanoribbons observed by TEM imaging (Figure 2f). The outer and inner diffused rings also supported the heterogeneity in the fibrillar structure.

CD and Fourier transform infrared (FTIR) spectra were used to demonstrate the molecular details of interstrand and intersheet interactions of the ribbons. As shown in Figure 4b, the negative and positive maximums at 225 and 206 nm, respectively, suggested a β-sheet structure. The negative peak was slightly red-shifted from the typical β-sheet absorbance at 218 nm, which was due to the aromatic interactions during peptide aggregation.[39−42] The FTIR spectrum obtained from freeze-dried peptide fibrils exhibited strong absorbance at 3285, 2955, and 2875 cm^{-1}, which corresponded to the N−H stretching, $-CH_3$ antisymmetric, and symmetric stretching,

DOI: 10.1021/acsnano.7b02325
ACS Nano 2017, 11, 8579−8589

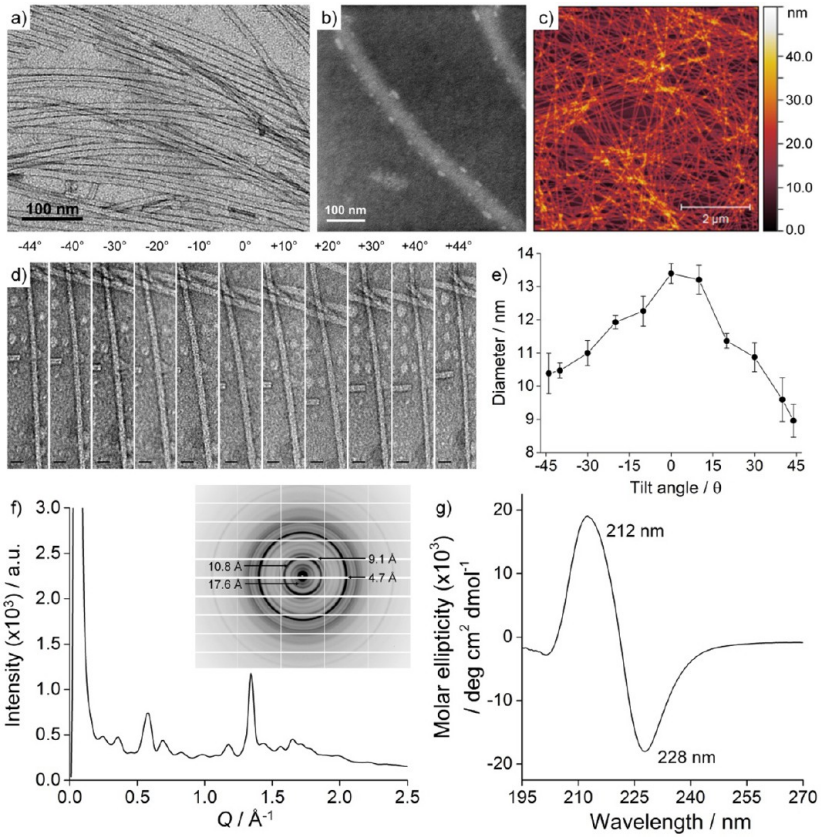

Figure 5. Structural characterization of Ac-NNFGAILTT ribbons by (a) TEM and (b) HAADF-STEM and (c) AFM imaging. (d,e) TEM images at different tilted angles (±44°) were obtained to confirm the planar structure of Ac-NNFGAILTT ribbons (scale bar: 20 nm). (e) Diameter of peptide ribbons was plotted against the tilting angles. (f) XRD analysis showing the diffraction pattern of the aligned peptide ribbons, in which the clear periodic rings implicated the highly crystallized structure. (g) CD spectrum showing the existence of β-sheet structure in the solution of Ac-NNFGAILTT.

respectively. Characteristic bands known as the amide I and II regions are located between 1700 and 1500 cm^{-1}, which are mainly due to the C═O and C−N stretching and N−H bending modes from amide groups of the peptide structure (Figure S7). The vibrational bands in the range of 1400 to 1300 cm^{-1} could likely be assigned to the C−N or C−O stretching and N−H bending modes of the peptide structure.[43] In particular, the strongest absorbance at 1628 cm^{-1} and the absence of 1690 cm^{-1} in the amide I region (Figure 4c) suggested a parallel β-sheet structure of the peptide fibrils.[44] Other pronounced vibrational bands displayed in the amide I (1667 and 1600 cm^{-1}) and amide II (1522 and 1516 cm^{-1}) regions confirmed a distinct β-sheet structure.[45] Based on these results, the 3D structure of the Ac-NNFGAILSS fibril was depicted using PyMol software (Figure 4d) and was consistent with the parallel, face-to-face β-sheets of NNFGAIL (21−27 residues)[31] and NFGAILS (22−28 residues) or FGAILSS (23−29 residues).[46]

Interestingly, untwisted structures (*i.e.*, planar ribbons) were observed for Ac-NNFGAILTT, where the C-terminal serine residues (Ser28, Ser29) of the Ac-NNFGAILSS segment were substituted by threonine. Analyses of TEM (Figure 5a,b) and AFM images (Figures 5c and S8) showed that the individual Ac-NNFGAILTT ribbon had a diameter of 8−10 nm and thickness of 9.4 nm. To confirm the morphology of Ac-NNFGAILTT ribbons, the peptide sample was imaged at a perpendicular orientation to the elongation axis of the ribbons before tilting between ±44°. As shown in Figure 5d,e, the ribbon thickness was reduced at higher angles, which indicated the planar ribbons instead of cylindrical structures. Compared to Ac-NNFGAILSS ribbons (Figure S4), long and untwisted ribbons of Ac-NNFGAILTT were observed immediately during the cooling process, showing a pronounced tendency for higher numbers of associated fibrils (Figure S9). As shown in Figure 5f, the XRD pattern showed a similar cross-β structure with the perpendicularly arranged meridional reflection at 4.7 Å and equatorial rings at 17.6, 10.8, and 9.1 Å. It was intriguing to find that the intersheet spacing of Ac-NNFGAILTT ribbons was smaller than the spacing obtained from Ac-NNFGAILSS (18.2 and 11.1 Å) and suggested the tighter intersheet contact. Additional rings in the equatorial region were reflections from higher-order periodicities, indicating that the Ac-NNFGAILTT ribbons possessed a highly crystallized structure. These reflection bands were difficult to assign, which was in part due to overlap with the diffused equatorial reflection from sample heterogeneity. The FTIR spectrum showed a similar interstrand peptide stacking as Ac-NNFGAILSS (Figure S10), in which the strongest absorbance at 1628 cm^{-1} and the absence of 1690 cm^{-1} suggested the parallel β-sheet structure of the ribbons. CD spectrum showed the β-sheet structure of Ac-NNFGAILTT ribbons, which exhibited both negative and positive peaks at 228 and 212 nm, respectively (Figure 5g). The larger red shift (Figure S11a) in the negative absorbance of the CD peak was observed in Ac-NNFGAILTT compared to Ac-NNFGAILSS (225 nm, Figure 4b), which confirmed a stronger intersheet aromatic interaction facilitated by the phenylalanine

DOI: 10.1021/acsnano.7b02325
ACS Nano 2017, 11, 8579−8589

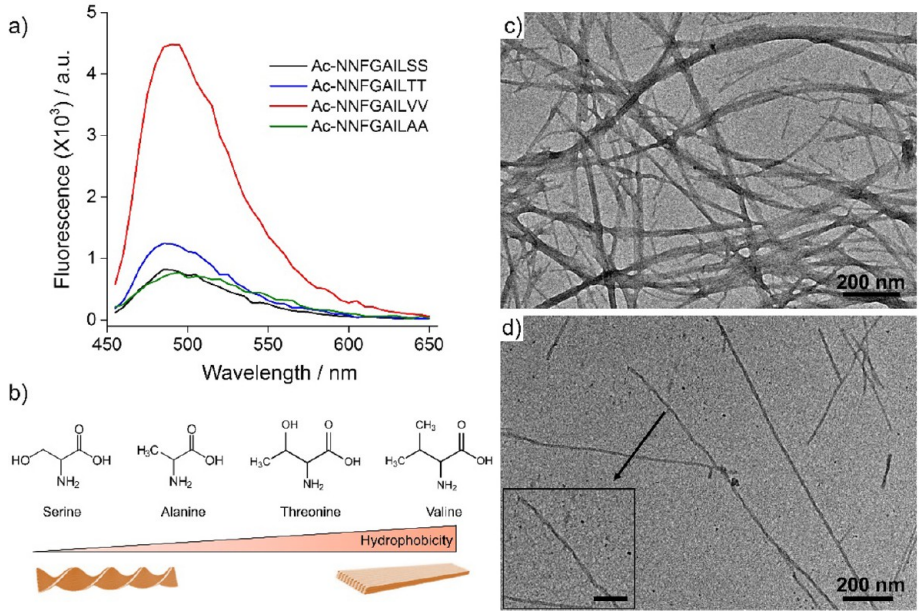

Figure 6. Effect of amino acid side chains on the peptide aggregation and fibril morphology. (a) ThT assay showing different strengths of β-sheet in the solution of Ac-NNFGAILSS, Ac-NNFGAILTT, Ac-NNFGAILVV, and Ac-NNFGAILAA. The peptide solutions (1.5 mM) were prepared in the phosphate buffer (20 mM, pH 7.5) containing 10 μM of ThT. The fluorescence measurements were performed at ex. 440 nm and em. 485 nm. (b) Schematic view showing fibril morphologies in relation to the hydrophobicity of amino acids. TEM images showed the highly aggregated, planar structures in the solution of Ac-NNFGAILVV (c) and nanoribbons in the solution of Ac-NNFGAILAA (d), in which twisted structures are indicated by the inset figure (scale bar: 100 nm).

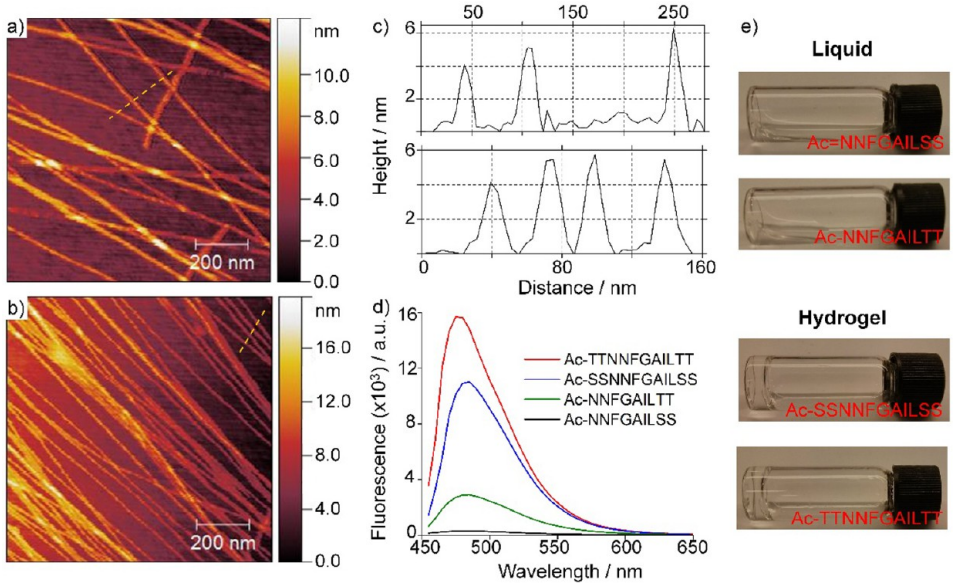

Figure 7. Effects of amino acid sequence on fibril morphologies, peptide aggregation, and hydrogelation behaviors. (a–c) AFM topographies of self-assembled nanoribbons: (a) Ac-SSNNFGAILSS and (b) Ac-TTNNFGAILTT. (c) Height profiles of the nanoribbons are shown along the dashed lines in the corresponding images (top: Ac-SSNNFGAILSS; bottom: Ac-TTNNFGAILTT). (d) ThT assay of the peptide solutions (2 mM), indicating the higher propensity of β-sheet formation for the extended peptides (ex. 440 nm and em. 485 nm). (e) Photos of the peptide solutions, in which hydrogelation was noted in the systems of extended peptide sequences (*i.e.*, Ac-SSNNFGAILSS and Ac-TTNNFGAILTT). The peptide solutions (5 mM) were aged in phosphate buffer (20 mM, pH 7.5) for 2 days before gel inversion test.

(Phe23) residue. The stronger β-sheet registry of Ac-NNFGAILTT was also confirmed by the ThT assay (Figure S11b), which showed an increased fluorescence intensity compared to that of Ac-NNFGAILSS.

The different morphologies of Ac-NNFGAILTT and Ac-NNFGAILSS fibrils were unexpected, given the high structure similarity of serine and threonine. We speculated that the presence of the methyl group in threonine of Ac-NNFGAILTT likely caused a restricted conformational freedom and stronger hydrophobic interactions that balanced the charge effect at the C-terminus. This was supported by XRD (Figures 4a and 5f) and CD data (Figures 4b and 5g), which suggested a reduced intersheet spacing and stronger main chain interactions by threonine substitution. AFM analyses (Figures 2d and S8b)

DOI: 10.1021/acsnano.7b02325
ACS Nano 2017, 11, 8579–8589

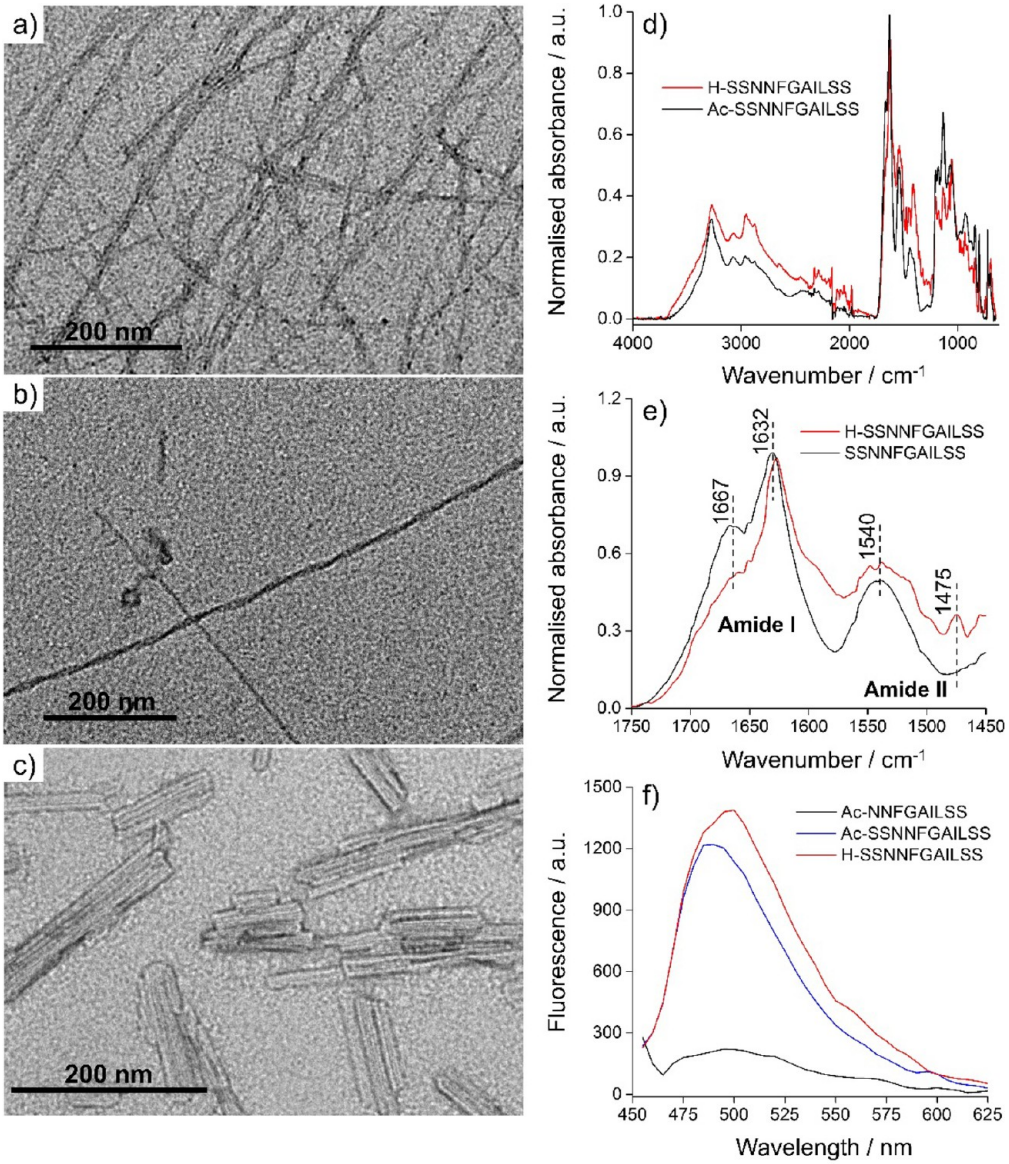

Figure 8. Effect of N-terminal capping on peptide aggregation and fibril morphology. TEM images of self-assembled peptide fibrils of (a,b) Ac-SSNNFGAILSS and (c) H-SSNNFGAILSS. Twisted fibrils were observed in (b). (d,e) FTIR spectra of Ac-SSNNFGAILSS and H-SSNNFGAILSS, labeling the peaks in the amide I and amide II regions, respectively. (f) ThT assay showing the different strengths of peptide β-sheet. The peptide solutions (2 mM) were prepared in the phosphate buffer (20 mM, pH 7.5) containing 10 μM of ThT. The fluorescence measurements were performed at ex. 440 nm and em. 485 nm.

showed an increased peptide stacking of Ac-NNFGAILTT over Ac-NNFGAILSS in the vertical direction, with the stronger lamination likely explaining the difficulty to introduce or maintain twisted structures. It was therefore proposed that the tighter β-sheet packing favored lateral associations into planar nanoribbons. The effect of serine and threonine side chains resulting in different biological products and conformations has been reported.[47−50] For example, studies by Martínez-Sáez and Corzana *et al.* showed striking differences in the ψ_s torsion angle depending on the glycosidic linkages with serine or threonine in the O-linked glycoproteins.[47,50] The former gave an alternate conformation (ψ_s = −97 or −180°), whereas the latter exhibited a rigid, eclipsed conformation at ψ_s = 63 or 120°, which was explained by the steric repulsion at the methyl group side chain of threonine.

We then further examined the side chain effects of the terminal residues on fibril formation. Peptide sequences with serine substitution by valine and alanine were synthesized separately, and fibril growth was performed under the same experimental conditions. ThT assay (Figure 6a) showed the varied aggregation propensity in the order: Ac-NNFGAILVV > Ac-NNFGAILTT > Ac-NNFGAILSS ≥ Ac-NNFGAILAA, which correlated with the twisted/untwisted morphologies. As proposed above and depicted in Figure 6b, stronger β-sheet registry led to untwisted ribbons of Ac-NNFGAILVV (Figure 6c) and Ac-NNFGAILTT (Figure 5a), whereas twisted fibrils were formed in Ac-NNFGAILSS (Figure 2a) and Ac-NNFGAILAA (Figure 6d). In particular, the aggregation propensity as determined by the ThT assay (Figure 6a) could correlate with the residue hydrophobicity, in which valine possessed the highest hydrophobicity while serine and alanine were more hydrophilic.[51−53] On the other hand, increased fibril thicknesses were noted in Ac-NNFGAILTT and Ac-NNFGAILVV, which was due to the enhanced side group

DOI: 10.1021/acsnano.7b02325
ACS Nano 2017, 11, 8579−8589

Table 1. Summary of the Peptide Sequences Investigated and the Corresponding β-Sheet Strength, Fibril Morphologies and Hydrogelation Relative to That of Ac-NNFGAILSS[a]

entry	property	sequence	morphology	aggregation tendency	hydrogelation
1	IAPP 21−29	Ac-NNFGAILSS	twisted	low	−
2	serine substitution	Ac-NNFGAILAA	twisted	low	−
3	serine substitution	Ac-NNFGAILTT	planar	medium	−
4	serine substitution	Ac-NNFGAILVV	planar	high	+
5	serine position shift	Ac-SSNNFGAIL	twisted	low	−
6	extended peptide	Ac-SSNNFGAILSS	partly twisted	high	+
7	extended peptide	Ac-TTNNFGAILTT	planar	high	+
8	uncapped peptide	H-SSNNFGAILSS	planar	high	+

[a]All the peptides were designed to possess the same amyloidogenic sequence NNFGAIL.

interaction that increased the peptide stacking in the vertical direction. Compared to Ac-NNFGAILTT, the Ac-NNFGAILVV fibrils exhibited an enhanced heterogeneity in fibril diameter. This could be due to the rapid aggregation of Ac-NNFGAILVV upon dissolving in the buffer and likely pre-existing oligomer seeds during peptide purification that accelerated the assembly process. The importance of C-terminal residues was also manifested by Ac-NNFGAIL where the two serine residues were removed from Ac-NNFGAILSS, and weak β-sheet formation was observed in this truncated sequence by ThT assay (Figure S12).

Extended peptide sequences with additional serine or threonine residues at the N-terminal region (*i.e.*, Ac-SSNNFGAILSS and Ac-TTNNFGAILTT) were next synthesized to study the intersheet molecular interactions and the resulting fibril structure. AFM height profiles (Figure 7a−d) showed the thickness of individual fibril was 4.5 and 4.8 nm for Ac-SSNNFGAILSS and Ac-TTNNFGAILTT, respectively. As confirmed by the ThT assay, the extended peptides exhibited stronger aggregation propensity and triggered water gelation due to the strengthened β-sheets (Figure 7d,e). To analyze the hydrogel properties, rheological studies were performed to determine the storage modulus (G') and loss modulus (G'') at varying frequencies of applied oscillatory stress, which correspond to the elastic and viscous responses of the peptide hydrogels, respectively. As shown in Figure S13, G' was higher than G'' in Ac-TTNNFGAILTT, indicating the elastic hydrogel formation. In line with the findings from Figures S4, S6, and 6a, substitution of serine with threonine enhanced the aggregation propensity of amyloid peptides (Figure S13c,d), leading to a higher value of G' for Ac-TTNNFGAILTT than Ac-SSNNFGAILSS (Figure S13d).

The Ac-TTNNFGAILTT fibrils were untwisted and had a diameter of 9.8 nm, which was likely a lateral association of two fibrils (Figure S14). Most Ac-SSNNFGAILSS fibrils also favored an untwisted structure (diameter: 8.5 nm), although some twisted fibrils were presented (Figure 8a,b). An uncapped peptide (H-SSNNFGAILSS) was prepared to examine the effect of charge interactions on peptide assembly, in which the opposite charges eliminated the electrostatic repulsions at the termini (Figure 8c). FTIR spectra show the parallel β-sheet structure for H-SSNNFGAILSS and Ac-SSNNFGAILSS (Figure 8d,e). The more defined FTIR peaks at 1540 cm^{-1} (amide II) and 1632 cm^{-1} (amide I) with the decreased absorbance at 1667 cm^{-1} (amide I) suggested the stronger order of the uncapped peptide fibrils. As shown by the TEM images in Figure 8c, the uncapped peptide boasted a marked difference from the capped sequence (Figure 8a) by exhibiting untwisted structures with strong lateral associations (*i.e.*, 4−10 or more associated fibrils). ThT assay showed an enhanced β-sheet formation of H-SSNNFGAILSS compared to the capped sequence (Figure 8f), which is due to the electrostatic attraction between $-NH_2$ and $-COOH$ that promoted peptide self-assembly into large nanostructures. The role of electrostatic interactions was also confirmed by adding salt to the Ac-SSNNFGAILSS solution to shield the terminal charge, in which an enhanced β-sheet formation was observed in the presence of higher concentrations (50 and 150 mM) of sodium chloride (NaCl) (Figure S15).

Finally, the serine residues of Ac-NNFGAILSS were shifted to the N-terminal region (Ac-SSNNFGAIL) to examine the effect of terminal serine residues. As shown in Figure S16, Ac-SSNNFGAIL exhibited a reduced aggregation propensity compared to Ac-NNFGAILSS, which indicated weaker interactions at Ser19 and Ser20 compared to the C-terminal serine. This observation was consistent with previous findings showing the important role of Ser28 to the fibrillation of IAPP (20−29, SNNFGAILSS) sequence.[30]

CONCLUSIONS

In summary, the fibrillation behaviors of eight IAPP-derived amyloidogenic peptides were systematically investigated, where the fibril structures/morphologies could be rationally tailored by varying the peptide sequences (Table 1). The IAPP 21−29 fragment (Ac-NNFGAILSS) aggregated into twisted ribbon-like structures, with the resultant diameter correlating with the number of associated fibrils. The spontaneous association of individual fibrils into larger twisted ribbons and superhelices was also observed. Increasing the β-sheet strength or intersheet contacts through additional H-bonds and/or hydrophobic interactions led to a reduction of torsional strain in the β-sheet and formation of untwisted planar ribbons. The ThT assay indicated a correlation between fibril morphology and β-sheet strength, in which untwisted planar structures displayed a stronger propensity to form β-sheets. This hypothesis was supported by amino acid substitution (*i.e.*, serine substitution by threonine, valine, and alanine), sequence elongation (*i.e.*, additional N-terminal serine and threonine), and terminal capping. The role of electrostatic interaction toward peptide assembly and the peptide sequence toward hydrogelation were also addressed. Since polymorphism is a common feature due to the variable amyloid fibril assembly pathways, and the fact that a correlation has been drawn between the fibril assembly/morphology and cellular toxicity,[54,55] we believe that our work will provide understanding of the amyloid-derived peptide self-assembly and the structural basis of amyloid polymorphism.

DOI: 10.1021/acsnano.7b02325
ACS Nano 2017, 11, 8579−8589

MATERIALS AND METHODS

Materials. Fmoc-protected amino acids for peptide synthesis were purchased from AGTC Bioproducts Ltd. Wang resins were used for peptide synthesis. Sodium phosphate monobasic (NaH_2PO_4), sodium phosphate dibasic (Na_2HPO_4), and Thioflavin T were purchased from Sigma-Aldrich (UK). Carbon grid (200 mesh copper) and uranyl acetate solution were purchased from Electron Microscopy Sciences. Milli-Q water (18.2 MΩ.cm) was used for all the experiments.

Solid Phase Peptide Synthesis. Peptides were synthesized by standard Fmoc chemistry using Wang resins. Protected amino acids were added to the growing peptide chain with the activating reagent 2-(1*H*-benzotriazol-1-yl)-1,1,3,3-tetramethyluronium hexafluorophosphate (HBTU). Following addition of the N-terminal amino acid, the Fmoc group was removed under 20% piperidine in DMF deprotection conditions. The peptides were cleaved by trifluoroacetic acid/triisopropylsilane/deionized water (95:2.5:2.5, v/v/v). The crude peptide was precipitated by cold ether several times, and reverse-phase high-performance liquid chromatography (HPLC, Shimadzu) was applied to obtain the target peptides. The Phenomenex C18 Gemini NX column was 150 × 21.2 mm and had a 5 μm pore size and 100 Å particle size.

Matrix-Assisted Desorption/Ionized Time-of-Flight Mass Spectrometry (MALDI-TOF MS). The purified and lyophilized peptide powders were dissolved in deionized water/acetonitrile (1:1, 2 mg/mL) and mixed 1:1 v/v with α-Cyano-4-hydroxycinnamic acid (CHCA) (8 mg/mL). The mixture was left to dry on the MS holder prior to MS analysis. MALDI-TOF (Micromass) was performed at reflection mode between 500 and 1800 *m*/*z*.

Preparation of Peptide Fibrils. Peptide powders were dissolved in sodium phosphate buffer (20 mM, pH 7.5) at desired concentrations. The solutions were heated to 70 °C for 10 min to fully dissolve the powders before being cooled at room temperature.

Transmission Electron Microscopy Imaging of Negative Stained Amyloid Fibrils. For TEM sample preparation, 10 μL of the aged fibril solution was dropped on a carbon film grid for 5 min, and the residual liquid was removed with a piece of filter paper. After that, the TEM grid was stained with 5 μL of 1 wt % uranyl acetate for 5 min. The excess staining agents were removed with filter papers. TEM imaging was performed on JEOL 2100F TEM with an acceleration voltage of 200 kV, and the images were recorded with an Orius camera. The fibril diameters, twist spacing, and twist angles were estimated from at least four measurements using ImageJ, depending on the fibril morphologies.

High-Resolution TEM/STEM Imaging of Unstained Amyloid Fibrils. TEM samples were prepared by dropping 10 μL of the aged fibril solution on an ultrathin carbon holey grid (400 mesh copper, Electron Microscopy Sciences) for 5 min, and the excess liquid was removed with filter paper. Electron microscopy characterizations of the unstained amyloid fibrils were performed on a Philips CM300 TEM at 300 kV and a Cs-corrected TEAM 0.5 TEM/STEM at 50 kV using a HAADF detector, which resulted in Z-contrast images.

X-ray Diffraction. Peptide solutions (25 mM) were prepared in phosphate buffer (20 mM, pH 7.5) and aged for at least 2 days prior to XRD sample preparation. The aged solution (10 μL) was dropped and suspended between two waxed stalks spaced around 2 cm. The droplet was left to dry at room temperature for at least 24 h. The diffraction pattern was collected at the Advanced Light Source Beamline 8.3.1 (λ = 1.12709 Å) with a Pilatus 6 M detector. Exposure times were 1.00 s with a 1.00° rotation at specimen-to detector distances of 350 mm. The 2D diffraction images were radially integrated into a 1D pattern by Nika 2D SAS software package for Igor Pro.[56]

Atomic Force Microscopy Imaging. For AFM sample preparation, 5−10 μL of the aged fibril solution was dropped on an oxygen plasma-treated silicon wafer (about 1 cm × 1 cm) for 5 min. The residual liquid was removed. AFM imaging was performed on a 5500 Microscope (Keysight Technologies, previously Agilent) in tapping mode in air. A HQ:NSC15/Al BS tip (μmasch) was applied for the topography imaging (tip radius of 8 nm, resonance frequency of 325 kHz, force constant of 40 N m^{-1}).

Circular Dichroism. Peptide solutions were prepared in phosphate buffer (20 mM, pH 7.5) and aged for at least 2 days prior to CD analyses. The samples were loaded in a 0.01 cm quartz cell, and CD measurement was performed with a Jasco-715 spectrometer, with the scanning speed of 100 nm/min, resolution of 2 nm, data pitch of 0.1 nm, accumulation time of 2, and response time of 4 s. The data unit was converted from machine units (millidegree, θ) into molar ellipticity $[\theta]$ using the equation

$$[\theta] = \theta/(10 \times P \times conc.)$$

where P is the path length in centimeters and *conc.* is the molar concentration of the peptide samples.

Fourier Transform Infrared Spectroscopy. The IR spectra of the fibril powders were obtained on FTIR spectrometry (Shimadzu) in attenuated total reflection mode, with the wavenumber scanned between 4000 and 650 cm^{-1}, response time of 8 s, and step of 1 cm^{-1}.

Thioflavin T Assay. To determine the critical aggregation concentration, different concentrations of peptide solutions were incubated with 10 μM of ThT in 384-well plates. The plate was left for at least 12 h at room temperature in the dark before fluorescence measurement. Fluorescence spectra were obtained on a PerkinElmer Enspire plate reader and SpectraMax M5 multimode microplate reader (Molecular Devices Ltd.) for Figure 7, with an excitation wavelength at 440 nm and emission between 455 and 700 nm. For measuring the kinetics of ThT fluorescence, peptide solutions (2 mM) were prepared in the phosphate buffer (20 mM, pH 7.5) containing 10 μM of ThT in 384-well plates prior to fluorescence measurement (ex. 440 nm, em. 485 nm).

Rheology. Peptide solutions (10 mM) were aged in phosphate buffer (20 mM, pH 7.5) for at least 2 days prior to the rheological measurement. Rheological properties were assessed using an Advanced Rheometer AR2000ex with AR Instrument Software (TA Instruments) fitted with a Peltier temperature control system. Oscillatory parallel plate rheological measurements were made at 25 °C using a 10 mm diameter steel plate with a 500 μm gap distance in the initial setup. The dynamic moduli of the peptide gels were obtained by measuring the G' and G'' as a function of controlled angular frequency in the range from 0.1 to 50 rad/s, with a constant strain value of 0.1%.

ASSOCIATED CONTENT

Supporting Information

The Supporting Information is available free of charge on the ACS Publications website at DOI: 10.1021/acsnano.7b02325.

HAADF-STEM, TEM, ThT assay, AFM, and FTIR characterizations of peptide fibrils (PDF)

AUTHOR INFORMATION

Corresponding Author

*E-mail: m.stevens@imperial.ac.uk.

ORCID

Michael R. Thomas: 0000-0001-7795-9648
Andy I. Nguyen: 0000-0003-4137-6453
E. Thomas Pashuck: 0000-0003-2881-4965
Ronald N. Zuckermann: 0000-0002-3055-8860
Molly M. Stevens: 0000-0002-7335-266X

Notes

The authors declare no competing financial interest.

ACKNOWLEDGMENTS

S.-T.W. thanks the financial support by Taiwan Strategic Alliance scholarship (UK-ICL-102-S03) and the Mobility Research Fellowship from the EPSRC Interdisciplinary Research Centre (IRC) "Early-Warning Sensing Systems for Infectious Diseases" (EP/K031953/1). M.M.S. and M.R.T. acknowledge support from the i-sense EPSRC IRC in Early

DOI: 10.1021/acsnano.7b02325
ACS Nano 2017, 11, 8579−8589

Warning Sensing Systems for Infectious Diseases (EP/K031953/1). M.M.S., Y.L., and E.T.P. acknowledge support from the ERC Seventh Framework Programme Consolidator grant "Naturale CG" (616417). M.M.S. acknowledges support from the Engineering and Physical Sciences Research Council grant "Bio-functionalized nanomaterials for ultrasensitive biosensing" (EP/K020641/1). N.A. was supported by Marie Curie actions FP7 through the Intra-European Marie Skłodowska-Curie Fellowship "ConPilus" (623123). P.A.P. was supported by the Australian Commonwealth Scientific and Industrial Research Organisation (CSIRO) in Manufacturing. S.C.S. acknowledges support from H2020 through the Individual Marie Skłodowska-Curie Fellowship "RADoTE" (701664). TEM imaging at the Molecular Foundry and X-ray diffraction experiments at the Advanced Light Source (Beamline 8.3.1), Lawrence Berkeley National Laboratory was supported by the Office of Science, Office of Basic Energy Sciences, of the U.S. Department of Energy under Contract No. DE-AC02-05CH11231. Research data is available online at DOI: 10.5281/zenodo.836641.

REFERENCES

(1) Dobson, C. M. Protein Misfolding, Evolution and Disease. *Trends Biochem. Sci.* **1999**, *24*, 329−332.
(2) Rochet, J. C.; Lansbury, P. T., Jr. Amyloid Fibrillogenesis: Themes and Variations. *Curr. Opin. Struct. Biol.* **2000**, *10*, 60−68.
(3) Glenner, G. G.; Ein, D.; Eanes, E. D.; Bladen, H. A.; Terry, W.; Page, D. L. Creation of "Amyloid" Fibrils from Bence Jones Proteins. *Science* **1971**, *174*, 712−714.
(4) Geddes, A. J.; Parker, K. D.; Atkins, E. D.; Beighton, E. "Cross-Beta" Conformation in Proteins. *J. Mol. Biol.* **1968**, *32*, 343−358.
(5) Nelson, R.; Sawaya, M. R.; Balbirnie, M.; Madsen, A. Ø.; Riekel, C.; Grothe, R.; Eisenberg, D. Structure of the Cross-β Spine of Amyloid-Like Fibrils. *Nature* **2005**, *435*, 773−778.
(6) Chiti, F.; Webster, P.; Taddei, N.; Clark, A.; Stefani, M.; Ramponi, G.; Dobson, C. M. Designing Conditions for *in Vitro* Formation of Amyloid Protofilaments and Fibrils. *Proc. Natl. Acad. Sci. U. S. A.* **1999**, *96*, 3590−3594.
(7) Hamley, I. W. The Amyloid Beta Peptide: A Chemist's Perspective. Role in Alzheimer's and Fibrillization. *Chem. Rev.* **2012**, *112*, 5147−5192.
(8) Petkova, A. T.; Leapman, R. D.; Guo, Z.; Yau, W. M.; Mattson, M. P.; Tycko, R. Self-Propagating, Molecular-Level Polymorphism in Alzheimer's β-Amyloid Fibrils. *Science* **2005**, *307*, 262−265.
(9) Adler-Abramovich, L.; Gazit, E. The Physical Properties of Supramolecular Peptide Assemblies: From Building Block Association to Technological Applications. *Chem. Soc. Rev.* **2014**, *43*, 6881−6893.
(10) Hamley, I. W. Peptide Fibrillization. *Angew. Chem., Int. Ed.* **2007**, *46*, 8128−8147.
(11) Gazit, E. Self Assembly of Short Aromatic Peptides into Amyloid Fibrils and Related Nanostructures. *Prion* **2007**, *1*, 32−35.
(12) Hu, Y.; Lin, R.; Zhang, P.; Fern, J.; Cheetham, A. G.; Patel, K.; Schulman, R.; Kan, C.; Cui, H. Electrostatic-Driven Lamination and Untwisting of β-Sheet Assemblies. *ACS Nano* **2016**, *10*, 880−888.
(13) Knowles, T. P.; Fitzpatrick, A. W.; Meehan, S.; Mott, H. R.; Vendruscolo, M.; Dobson, C. M.; Welland, M. E. Role of Intermolecular Forces in Defining Material Properties of Protein Nanofibrils. *Science* **2007**, *318*, 1900−1903.
(14) López de la Paz, M.; Goldie, K.; Zurdo, J.; Lacroix, E.; Dobson, C. M.; Hoenger, A.; Serrano, L. *De Novo* Designed Peptide-Based Amyloid Fibrils. *Proc. Natl. Acad. Sci. U. S. A.* **2002**, *99*, 16052−16057.
(15) López de la Paz, M.; Serrano, L. Sequence Determinants of Amyloid Fibril Formation. *Proc. Natl. Acad. Sci. U. S. A.* **2004**, *101*, 87−92.
(16) Bertolani, A.; Pirrie, L.; Stefan, L.; Houbenov, N.; Haataja, J. S.; Catalano, L.; Terraneo, G.; Giancane, G.; Valli, L.; Milani, R.; et al. Supramolecular Amplification of Amyloid Self-Assembly by Iodination. *Nat. Commun.* **2015**, *6*, 7574.
(17) Castelletto, V.; Hamley, I. W.; Hule, R. A.; Pochan, D. Helical-Ribbon Formation by a Beta-Amino Acid Modified Amyloid β-Peptide Fragment. *Angew. Chem., Int. Ed.* **2009**, *48*, 2317−2320.
(18) Lu, K.; Jacob, J.; Thiyagarajan, P.; Conticello, V. P.; Lynn, D. G. Exploiting Amyloid Fibril Lamination for Nanotube Self-Assembly. *J. Am. Chem. Soc.* **2003**, *125*, 6391−6393.
(19) Benzinger, T. L. S.; Gregory, D. M.; Burkoth, T. S.; Miller-Auer, H.; Lynn, D. G.; Botto, R. E.; Meredith, S. C. Two-Dimensional Structure of β-Amyloid(10−35) Fibrils. *Biochemistry* **2000**, *39*, 3491−3499.
(20) Liang, Y.; Pingali, S. V.; Jogalekar, A. S.; Snyder, J. P.; Thiyagarajan, P.; Lynn, D. G. Cross-Strand Pairing and Amyloid Assembly. *Biochemistry* **2008**, *47*, 10018−10026.
(21) Swanekamp, R. J.; DiMaio, J. T. M.; Bowerman, C. J.; Nilsson, B. L. Coassembly of Enantiomeric Amphipathic Peptides into Amyloid-Inspired Rippled β-Sheet Fibrils. *J. Am. Chem. Soc.* **2012**, *134*, 5556−5559.
(22) Cui, H.; Cheetham, A. G.; Pashuck, E. T.; Stupp, S. I. Amino Acid Sequence in Constitutionally Isomeric Tetrapeptide Amphiphiles Dictates Architecture of One-Dimensional Nanostructures. *J. Am. Chem. Soc.* **2014**, *136*, 12461−12468.
(23) Tsemekhman, K.; Goldschmidt, L.; Eisenberg, D.; Baker, D. Cooperative Hydrogen Bonding in Amyloid Formation. *Protein Sci.* **2007**, *16*, 761−764.
(24) Doran, T. M.; Kamens, A. J.; Byrnes, N. K.; Nilsson, B. L. Role of Amino Acid Hydrophobicity, Aromaticity, and Molecular Volume on Iapp(20−29) Amyloid Self-Assembly. *Proteins: Struct., Funct., Genet.* **2012**, *80*, 1053−1065.
(25) Cinar, G.; Orujalipoor, I.; Su, C.-J.; Jeng, U. S.; Ide, S.; Guler, M. O. Supramolecular Nanostructure Formation of Coassembled Amyloid Inspired Peptides. *Langmuir* **2016**, *32*, 6506−6514.
(26) Lakshmanan, A.; Cheong, D. W.; Accardo, A.; Di Fabrizio, E.; Riekel, C.; Hauser, C. A. E. Aliphatic Peptides Show Similar Self-Assembly to Amyloid Core Sequences, Challenging the Importance of Aromatic Interactions in Amyloidosis. *Proc. Natl. Acad. Sci. U. S. A.* **2013**, *110*, 519−524.
(27) Telling, G. C.; Parchi, P.; DeArmond, S. J.; Cortelli, P.; Montagna, P.; Gabizon, R.; Mastrianni, J.; Lugaresi, E.; Gambetti, P.; Prusiner, S. B. Evidence for the Conformation of the Pathologic Isoform of the Prion Protein Enciphering and Propagating Prion Diversity. *Science* **1996**, *274*, 2079−2082.
(28) Sanke, T.; Bell, G. I.; Sample, C.; Rubenstein, A. H.; Steiner, D. F. An Islet Amyloid Peptide Is Derived from an 89-Amino Acid Precursor by Proteolytic Processing. *J. Biol. Chem.* **1988**, *263*, 17243−17246.
(29) Glenner, G. G.; Eanes, E. D.; Wiley, C. A. Amyloid Fibrils Formed from a Segment of the Pancreatic Islet Amyloid Protein. *Biochem. Biophys. Res. Commun.* **1988**, *155*, 608−614.
(30) Westermark, P.; Engström, U.; Johnson, K. H.; Westermark, G. T.; Betsholtz, C. Islet Amyloid Polypeptide: Pinpointing Amino Acid Residues Linked to Amyloid Fibril Formation. *Proc. Natl. Acad. Sci. U. S. A.* **1990**, *87*, 5036−5040.
(31) Wiltzius, J. J. W.; Sievers, S. A.; Sawaya, M. R.; Cascio, D.; Popov, D.; Riekel, C.; Eisenberg, D. Atomic Structure of the Cross-β Spine of Islet Amyloid Polypeptide (Amylin). *Protein Sci.* **2008**, *17*, 1467−1474.
(32) Goldsbury, C. S.; Cooper, G. J.; Goldie, K. N.; Muller, S. A.; Saafi, E. L.; Gruijters, W. T.; Misur, M. P.; Engel, A.; Aebi, U.; Kistler, J. Polymorphic Fibrillar Assembly of Human Amylin. *J. Struct. Biol.* **1997**, *119*, 17−27.
(33) Aggeli, A.; Nyrkova, I. A.; Bell, M.; Harding, R.; Carrick, L.; McLeish, T. C. B.; Semenov, A. N.; Boden, N. Hierarchical Self-Assembly of Chiral Rod-Like Molecules as a Model for Peptide β-Sheet Tapes, Ribbons, Fibrils, and Fibers. *Proc. Natl. Acad. Sci. U. S. A.* **2001**, *98*, 11857−11862.
(34) Aggeli, A.; Bell, M.; Carrick, L. M.; Fishwick, C. W. G.; Harding, R.; Mawer, P. J.; Radford, S. E.; Strong, A. E.; Boden, N. Ph as a

DOI: 10.1021/acsnano.7b02325
ACS Nano 2017, 11, 8579−8589

Trigger of Peptide β-Sheet Self-Assembly and Reversible Switching between Nematic and Isotropic Phases. *J. Am. Chem. Soc.* **2003**, *125*, 9619−9628.
(35) Hall, D. M.; Bruss, I. R.; Barone, J. R.; Grason, G. M. Morphology Selection *Via* Geometric Frustration in Chiral Filament Bundles. *Nat. Mater.* **2016**, *15*, 727−732.
(36) Muraoka, T.; Cui, H.; Stupp, S. I. Quadruple Helix Formation of a Photoresponsive Peptide Amphiphile and Its Light-Triggered Dissociation into Single Fibers. *J. Am. Chem. Soc.* **2008**, *130*, 2946−2947.
(37) Pashuck, E. T.; Stupp, S. I. Direct Observation of Morphological Tranformation from Twisted Ribbons into Helical Ribbons. *J. Am. Chem. Soc.* **2010**, *132*, 8819−8821.
(38) Perutz, M. F.; Finch, J. T.; Berriman, J.; Lesk, A. Amyloid Fibers Are Water-Filled Nanotubes. *Proc. Natl. Acad. Sci. U. S. A.* **2002**, *99*, 5591−5595.
(39) Ma, S.; Shen, S.; Lee, H.; Eriksson, M.; Zeng, X.; Xu, J.; Fandrick, K.; Yee, N.; Senanayake, C.; Grinberg, N. Mechanistic Studies on the Chiral Recognition of Polysaccharide-Based Chiral Stationary Phases Using Liquid Chromatography and Vibrational Circular Dichroism: Reversal of Elution Order of N-Substituted Alpha-Methyl Phenylalanine Esters. *J. Chromatogr. A* **2009**, *1216*, 3784−3793.
(40) Nishio, M.; Hirota, M.; Umezawa, Y. *The CH/Π Interaction: Evidence, Nature, and Consequences*; John Wiley & Sons, 1998.
(41) Roy, R. S.; Gopi, H. N.; Raghothama, S.; Gilardi, R. D.; Karle, I. L.; Balaram, P. Peptide Hairpins with Strand Segments Containing α- and β-Amino Acid Residues: Cross-Strand Aromatic Interactions of Facing Phe Residues. *Biopolymers* **2005**, *80*, 787−799.
(42) Castelletto, V.; Hamley, I. W.; Harris, P. J.; Olsson, U.; Spencer, N. Influence of the Solvent on the Self-Assembly of a Modified Amyloid Beta Peptide Fragment. I. Morphological Investigation. *J. Phys. Chem. B* **2009**, *113*, 9978−9987.
(43) Sevinc, A.; Yonar, D.; Severcan, F. Investigation of Neuro-degenerative Diseases from Body Fluid Samples Using Fourier Transform Infrared Spectroscopy. *Biomed. Spectrosc. Imaging* **2015**, *4*, 341−357.
(44) Madine, J.; Jack, E.; Stockley, P. G.; Radford, S. E.; Serpell, L. C.; Middleton, D. A. Structural Insights into the Polymorphism of Amyloid-Like Fibrils Formed by Region 20−29 of Amylin Revealed by Solid-State Nmr and X-Ray Fiber Diffraction. *J. Am. Chem. Soc.* **2008**, *130*, 14990−15001.
(45) Buchanan, L. E.; Dunkelberger, E. B.; Tran, H. Q.; Cheng, P.-N.; Chiu, C.-C.; Cao, P.; Raleigh, D. P.; de Pablo, J. J.; Nowick, J. S.; Zanni, M. T. Mechanism of Iapp Amyloid Fibril Formation Involves an Intermediate with a Transient β-Sheet. *Proc. Natl. Acad. Sci. U. S. A.* **2013**, *110*, 19285−19290.
(46) Soriaga, A. B.; Sangwan, S.; Macdonald, R.; Sawaya, M. R.; Eisenberg, D. Crystal Structures of Iapp Amyloidogenic Segments Reveal a Novel Packing Motif of out-of-Register Beta Sheets. *J. Phys. Chem. B* **2016**, *120*, 5810−5816.
(47) Corzana, F.; Busto, J. H.; Jimenez-Oses, G.; Garcia de Luis, M.; Asensio, J. L.; Jimenez-Barbero, J.; Peregrina, J. M.; Avenoza, A. Serine *Versus* Threonine Glycosylation: The Methyl Group Causes a Drastic Alteration on the Carbohydrate Orientation and on the Surrounding Water Shell. *J. Am. Chem. Soc.* **2007**, *129*, 9458−9467.
(48) Tachibana, Y.; Fletcher, G. L.; Fujitani, N.; Tsuda, S.; Monde, K.; Nishimura, S.-I. Antifreeze Glycoproteins: Elucidation of the Structural Motifs That Are Essential for Antifreeze Activity. *Angew. Chem.* **2004**, *116*, 874−880.
(49) Kang, M. K.; Colombo, J. S.; D'Souza, R. N.; Hartgerink, J. D. Sequence Effects of Self-Assembling Multidomain Peptide Hydrogels on Encapsulated Shed Cells. *Biomacromolecules* **2014**, *15*, 2004−2011.
(50) Martínez-Sáez, N.; Castro-López, J.; Valero-González, J.; Madariaga, D.; Compañón, I.; Somovilla, V. J.; Salvadó, M.; Asensio, J. L.; Jiménez-Barbero, J.; Avenoza, A.; et al. Deciphering the Non-Equivalence of Serine and Threonine O-Glycosylation Points: Implications for Molecular Recognition of the Tn Antigen by an Anti-Muc1 Antibody. *Angew. Chem., Int. Ed.* **2015**, *54*, 9830−9834.
(51) Eisenberg, D.; Weiss, R. M.; Terwilliger, T. C.; Wilcox, W. Hydrophobic Moments and Protein Structure. *Faraday Symp. Faraday Symp. Chem. Soc.* **1982**, *17*, 109−120.
(52) Cornette, J. L.; Cease, K. B.; Margalit, H.; Spouge, J. L.; Berzofsky, J. A.; DeLisi, C. Hydrophobicity Scales and Computational Techniques for Detecting Amphipathic Structures in Proteins. *J. Mol. Biol.* **1987**, *195*, 659−685.
(53) Eisenberg, D.; Schwarz, E.; Komaromy, M.; Wall, R. Analysis of Membrane and Surface Protein Sequences with the Hydrophobic Moment Plot. *J. Mol. Biol.* **1984**, *179*, 125−142.
(54) Kreplak, L.; Aebi, U. From the Polymorphism of Amyloid Fibrils to Their Assembly Mechanism and Cytotoxicity. *Adv. Protein Chem.* **2006**, *73*, 217−233.
(55) Seilheimer, B.; Bohrmann, B.; Bondolfi, L.; Müller, F.; Stüber, D.; Döbeli, H. The Toxicity of the Alzheimer's β-Amyloid Peptide Correlates with a Distinct Fiber Morphology. *J. Struct. Biol.* **1997**, *119*, 59−71.
(56) Ilavsky, J. Nika: Software for Two-Dimensional Data Reduction. *J. Appl. Crystallogr.* **2012**, *45*, 324−328.

DOI: 10.1021/acsnano.7b02325
ACS Nano 2017, 11, 8579−8589